Front. Phys. China, 2008, 3(2): 165–172
DOI 10.1007/s11467-008-0019-x

REVIEW ARTICLE

Wei CHENG, David MARX, Shang-fen REN

Microscopic phonon theory of Si/Ge nanocrystals

Abstract Microscopic phonon theory of semiconductor nanocrystals (NCs) is reviewed in this paper. Phonon modes of Si and Ge NCs with various sizes of up to 7 nm are investigated by valence force field theory. Phonon modes in spherical SiGe alloy NCs approximately 3.6 nm (containing 1147 atoms) in size have been investigated as a function of the Si concentration. Phonon density-of-states, quantum confinement effects, as well as Raman intensities are discussed.

Keywords semiconductor nanocrystal, alloy, phonon, lattice dynamics, Raman

PACS numbers 81.05.Cy, 81.05.Bx, 63.22.+m, 63.50.+x, 78.30.-j

1 Introduction

SiGe has rich applications in high-speed inexpensive devices and has received plenty of interest in recent years [1]. Many optical, transport, and thermal properties of nanocrystals (NCs) are related to phonon properties [2–4]. Phonon properties of NCs are becoming more important. One kind of thermoelectric material is Si and Ge NCs [5–7]. The increase in the figure of merit is mainly related to the minimization of thermal conductivity of phonons [6, 7]. Currently, most of the theoretical understanding of phonon modes in NCs is based on continuum dielectric models [8–10]. However, one of the basic assumptions of all dielectric models is that the material is homogeneous and isotropic, i.e., only valid in the long wavelength limit. When the size of NCs is small, in the range of a few nm, the continuum dielectric models are intrinsically limited. In recent years, we have developed a microscopic valence force field model (VFFM) [11] to study phonon modes in NCs [7, 12–19].

Raman spectroscopy is a powerful tool to detect phonon properties in Si/Ge NCs. Quantum confinement effects as well as matrix effects can be detected in Raman spectra. Raman spectra of ultra-thin Ge film grown on Si [100] surface [20], Ge/Si superlattice [21], and self-organized Ge quantum dots superlattice grown on Si substrates [22] have been reported. Raman spectra of Si, Ge, and SiGe alloy NCs can be calculated by bond-charge approximation [12, 23]. In this paper, we review briefly some of the phonon-related properties of Si, Ge and SiGe alloy NCs in microscopic phonon theory. The calculated spectra are compared with available experiments.

Wei CHENG[1, 2], David MARX[2], Shang-fen REN[2] (✉)

[1] Key Laboratory in University for Radiation Beam Technology and Materials Modification, Institute of Low Energy Nuclear Physics, Beijing Normal University, Beijing 100875, China

[2] Department of Physics, Illinois State University, Normal, IL 61790-4560, USA

E-mail: ren@phy.ilstu.edu

Received February 26, 2008; accepted March 8, 2008

2 Valence force field model (VFFM)

The microscopic VFFM used in calculations of NC phonons has been described in detail in publications [11, 12]. The potential energy difference ΔE in the VFFM for bond stretching and bond angle bending is

$$\Delta E = \sum_i C_0(\Delta b_i/b)^2/2 + \sum_j C_1(\Delta\theta_j)^2/2 \qquad (1)$$

where the two force constants are chosen to be $C_0 = 49.1$ eV, $C_1 = 1.07$ eV for Si, and $C_0 = 47.2$ eV, $C_1 = 0.845$ eV for Ge [11]. The first summation is over all the bonds i of equilibrium length b, while the second summation is over all the bond angles j. In the alloys, there are Si-Si, Si-Ge, and Ge-Ge bonds. The force constants

of all bonds are assumed to be the same as Ge. The Si and Ge masses are taken as 28.09 and 72.59 atomic units, respectively. The highest Si bulk optical phonon frequency calculated in this mass-difference approximation is 502 cm^{-1}, which differs from the experimental value of 520 cm^{-1} by only 3 %. This suggests that the mass-approximation used in the calculations is reasonably good. From Eq. (1), the dynamical matrix can be constructed for a Si/Ge NC. The assumption that the Si/Ge NC is symmetrical enables the use of group theory to reduce the dimension of the dynamical matrix. By solving the dynamical matrix, the frequencies as well as eigenvectors of phonon modes are obtained.

3 Phonon density of states of Ge NCs

The Ge NCs in our calculations are spherical and of T_d symmetry. The spherical NCs are constructed in the following manner: The smallest NC has five atoms, with one inner atom surrounded by four nearest atoms. The next larger NC has 17 atoms, with each of the four outer atoms surrounded by another three atoms. Other larger NCs are constructed by adding spherical layers of atoms one by one in the same manner. The highest possible point group T_d symmetry of these Ge NCs allows us to calculate phonons of NCs with diameter of up to 7 nm (8105 Atoms). In our investigations, we calculated phonon modes in Ge NCs with two different types of surfaces (free standing surface and fixed surface) in the size range from five atoms up to about 7 nm in diameter [13]. Realistic NCs are usually embedded in a matrix with boundary conditions between the above two surfaces. The phonon density of states [PDOS $D(\omega)$] of Ge NCs with the two types of surfaces and a few sizes are shown in Fig. 1. The left panel is for Ge NCs with a fixed surface, while the right panel is for Ge NCs with a free surface. Comparing these results, it is observed that there are more low frequency peaks in Ge NCs with a free surface than in Ge NCs with a fixed surface. As the size of the Ge NCs increases, the frequency of the highest optical modes is blue-shifted. This is indicative of the quantum confinement effect as discussed in Ref. [12]. This is particularly obvious when the nanocrystal diameter is less than 3 nm. When the size of Ge NCs increases up to 7 nm, the PDOS of Ge NCs with these two different surfaces both approach that of the bulk. One major feature of phonons in Ge NCs with a fixed surface is that there is always a major peak at the frequency of about 211 cm^{-1}, which corresponds to the frequency range between the optical and acoustic phonons of the bulk Ge. This peak represents interface phonons, which are still strong in Ge NCs of 7 nm, or the maximum size of our present calculations.

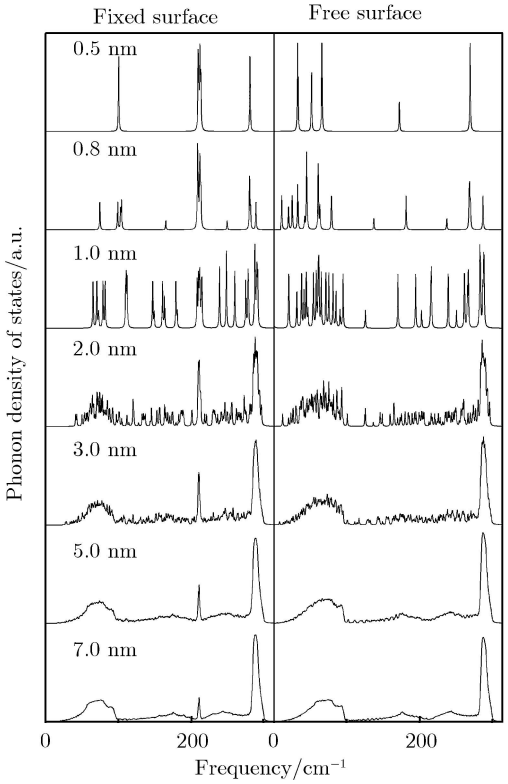

Fig. 1 Calculated total phonon DOS for Ge QDs, with fixed or free surfaces of approximate sizes/diameters indicated in nm.

4 Phonon density of states of Si_xGe_{1-x} NCs

Phonon modes of Si NCs follow similar rules as Ge NCs discussed above [12, 13]. The PDOS of spherical Si_xGe_{1-x} alloy NCs containing a total of 1147 atoms (diameter d ~3.7 nm for pure Ge and d ~3.5 nm for pure Si) with varying fractions of Si is shown in Fig. 2. In our calculations, we assume that the Si atoms are randomly distributed within the NC, and there is no ordering of any type in the NCs. In particular, there is no long-range ordering of the Si and Ge atoms which has been found experimentally to give rise to well-defined Raman peaks of around 255 and 435 cm^{-1}[24]. The force constant parameters of the Si_xGe_{1-x} are chosen the same way as the Ge parameters [15]. Since Si and Ge bulk materials have different lattice constants, the lattice constant of the alloy Si_xGe_{1-x} is approximated by an interpolation between those of Si and Ge using Vegard's law [25], $a = xa_{\rm Si} + (1-x)a_{\rm Ge}$, where $a_{\rm Si}$ and $a_{\rm Ge}$ are the lattice constants of Si and Ge respectively, and x is the silicon fractional concentration. We typically start from a small NC that is approximately spherical in shape.

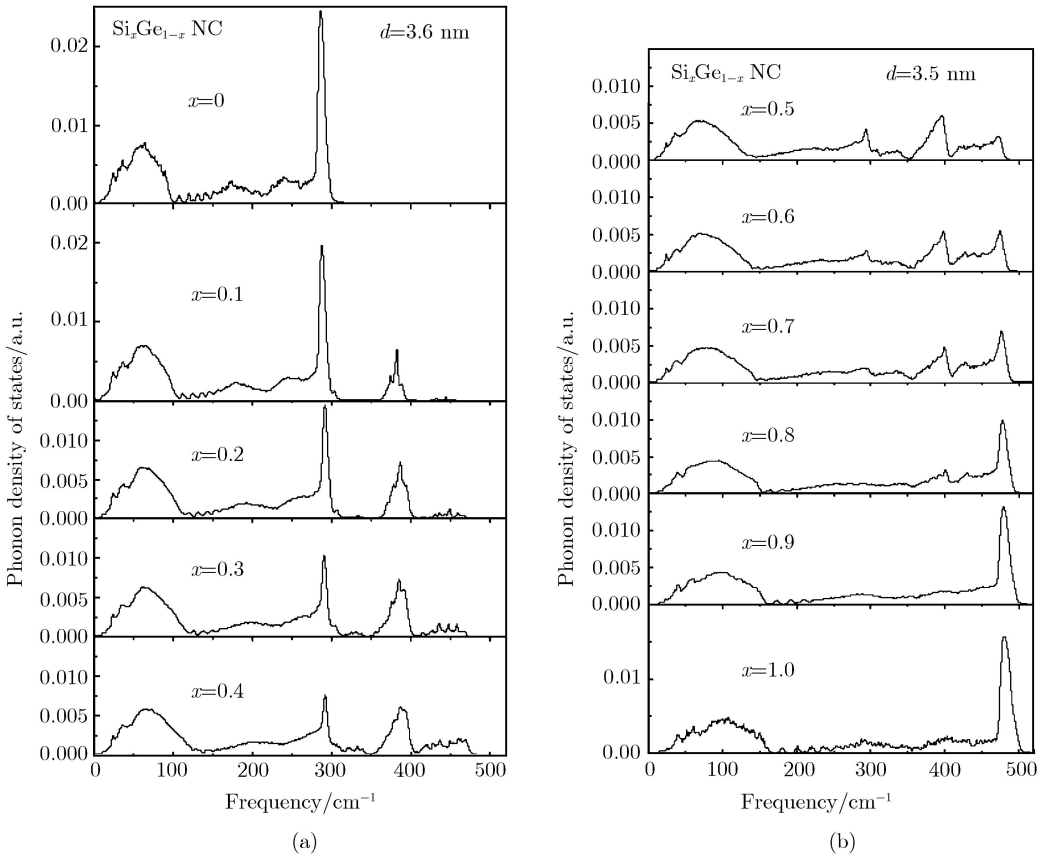

Fig. 2 The calculated phonon density-of-states (PDOS) in spherical SiGe NC with total number of atoms N=1147, $d \sim$ 3.6 nm for Si concentration x equal to **(a)** 0 to 0.4 and **(b)** 0.5 to 1.

The numbers of Si and Ge atoms are fixed and the computer programs are run many times with random locations of the Si atoms. Our results show that when the NC is small, the PDOS depends on the location of the Si atoms. However, as the size of the NC becomes large enough, the PDOS of the alloy will "stabilize" and become independent of the distribution of the Si atoms.

As shown in Fig. 2, there are two acoustic peaks at approximately 24 and 38 cm^{-1} for x <0.8. They correspond to spheroidal and torsional Lamb modes [14–17, 26]. However, when x becomes 0.8, they are replaced by two peaks with frequencies equal to 38 and 60 cm^{-1}. These results suggest that the dependence of the two Lamb modes on the alloy composition in SiGe NC is similar to the "two-mode behavior" of optical phonons in bulk alloys [27].

The bulk Ge optical phonon region is around 300 cm^{-1}, the bulk Si optical phonon region around 500 cm^{-1}, and the "so-called" Si-Ge vibration region around 400 cm^{-1}. The Ge optical peak blue-shifts slightly as x increases. The decrease in strength agrees with the experimental measurements [28, 29]. The experimental Ge phonon peak frequency in the bulk alloy shows a red-shift with an increase in x rather than the slight blue-shift predicted by our calculations. Two factors influence the frequency of this peak in our understanding. First, the contraction of the Si-Ge alloy lattice constant by Vegard's law would cause a blue-shift of the peak. Second, the increasing localization of Ge optical modes due to the increasing amount of Si would cause a red-shift of this peak.

5 Localized and delocalized modes in Si$_x$ Ge$_{1-x}$ NCS

We want to investigate the vibration details of a single phonon mode, including whether it is a localized mode or spread in the NC, whether it is a surface mode or a body mode, and the frequency range of the mode. We thus introduce a quantity as vibration amplitude squared (VAS), of which the sum of all atoms is normalized to one. From the calculated VAS of each mode, we can select the single atom that has the maximum value of VAS (to be abbreviated as MVAS) and plot the MVAS as a function of the phonon frequencies. If the MVAS of one mode is close to unity, this mode must be highly

localized, since this indicates that only one atom vibrates very strongly at this frequency and all the other atoms are almost still. Conversely, if the MVAS is significantly less than 1, it implies a large number of atoms involved in the vibration of this mode. In particular, if the MVAS is close to the inverse of the number of atoms in the NC, it indicates that all the atoms in the NC have nearly the same vibration amplitudes. Such plots have been shown to be useful in studying surface vibrational modes of NC as distinct from those involving atoms lying in the interior.

In case of a binary alloy Si_xGe_{1-x} NCs, we have separately plotted the MVAS for the two different types of atoms (Si or Ge) present in the alloy to highlight their different behaviors. Examples of such plots are shown in Fig. 3 for Si_xGe_{1-x} NCs with alloy compositions x=0.1. In the low frequency range there are two sharp localized Ge peaks. These are also surface acoustic phonon peaks as discussed in the next paragraph. We found that as x changes in the alloy NC, the frequencies of these surface acoustic phonons remain more or less the same as those of the pure Ge NC until x reaches 0.7. There is also no obvious change in the widths and heights of those two peaks as shown in Fig. 2. In the high frequency region above 300 cm^{-1}, all the modes are Si major localized modes.

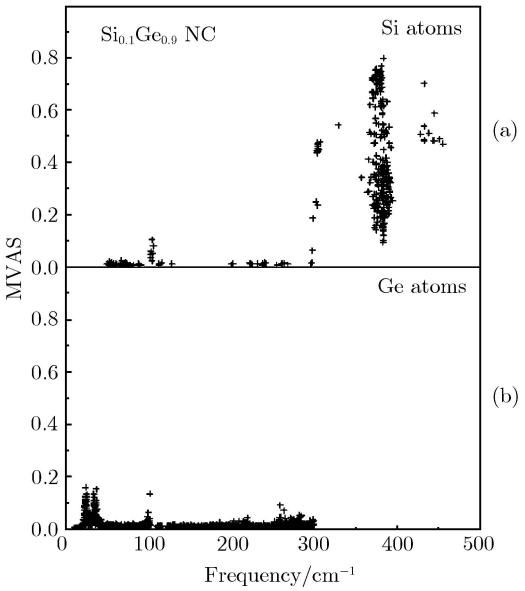

Fig. 3 Plot of the displacement amplitude-squared (AS) of the atom whose value of AS has the maximum value (or MVAS) versus the mode frequency for the alloy $Si_{0.1}Ge_{0.9}$. The atoms are further separated according to whether they are **(a)** Si or **(b)** Ge atoms.

In Fig. 4 the MVAS of the Si and Ge atoms in the same alloys are separated according to their different locations, with surface atoms as opposites to "body" atoms lying in the interior of the NC. In this paper we have defined surface atoms as atoms containing at least one dangling bond. In the low frequency region the two peaks are found to be localized surface phonon peaks. In the high frequency region the peak of surface modes red-shifts for the same SiGe modes at 400 cm^{-1}.

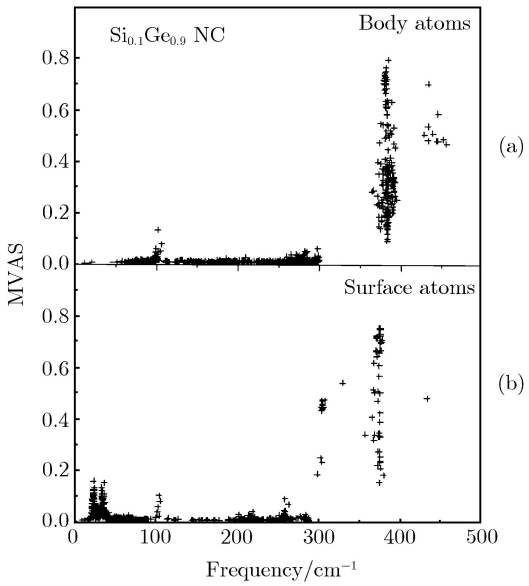

Fig. 4 Plot of the displacement amplitude-squared (AS) of the atom whose value of AS has the maximum value (or MVAS) versus the mode frequency for the alloy $Si_{0.1}Ge_{0.9}$. The atoms are further separated according to whether they are **(a)** body or **(b)** surface atoms.

In Fig. 5 the MVAS of both Si and Ge atoms are further separated according to their nearest neighbor configurations to investigate the relation between the vibration frequency of an atom and its local environment. Each interior atom, whether Si or Ge, has four nearest neighbors, so each atom with the MVAS can have up to five different combinations of nearest neighbor atoms. For example, if the center atom is Si, its four nearest neighboring atoms can have zero to four Si atoms, or four to zero Ge atoms. It should be noted that we have treated only interior atoms here, i.e., the summation of all the MVAS in Fig. 5 should be equal to the upper panel of Fig. 4. The lower panels of Fig. 4 which correspond to the MVAS of surface atoms (which have at least one dangling bond) are not included in Fig. 5. In the PDOS, for x <0.8, there are two sharp peaks in the low frequency region. When the concentration of Si is low, they are modes of Ge major localized surface modes as shown in Figs. 3 and 4. When x increases, a part of the surface modes become Si major localized modes. Within the limit when the NC size becomes large, these surface modes become the torsional and spheroidal distortion modes of a homogeneous sphere predicted theoretically by Lamb [26]. The

NC size d ∼3.6 nm in the present study is near the NC size limit where the Lamb theory is still valid [14, 16, 17]. The peak at 100 cm^{-1} is mostly localized modes with a Ge at center surrounded by three Si and one Ge (Ge-Si_3Ge) atoms. The peak at 400 cm^{-1} is mostly localized modes with configurations (Si-Ge_4). The peak at 450 cm^{-1} is mostly localized modes with configurations (Si-$SiGe_3$, Si-Si_2Ge_2).

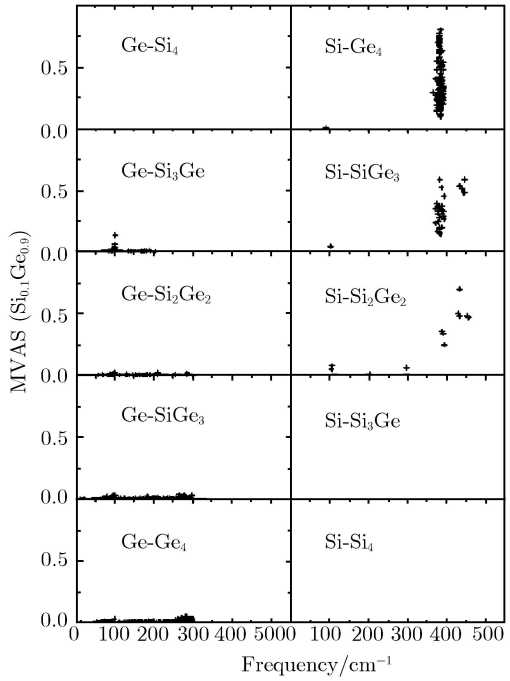

Fig. 5 Plot of the displacement amplitude-squared (AS) of the atom whose value of AS has the maximum value (or MVAS) versus the mode frequency for the alloy $Si_{0.1}Ge_{0.9}$. The atoms are separated according to whether they are Ge or Si atoms. The left-hand side column shows the Ge atoms surrounded by different numbers of Ge atoms, while the right-hand side column shows the Si atoms surrounded by different numbers of Ge atoms.

6 Raman intensities of Si and Ge NCs

Raman intensities can be calculated by bond-polarizable approximation [23]. We have calculated Raman intensities of Si NCs with free surfaces and approximate diameters between 1.5 to 7.6 nm in T_d symmetry [12]. Raman intensity of each irreducible mode is obtained. The final Raman intensity of the whole Si NC can be calculated by the Lorentz broadening of all the modes. Our Si NCs have a spherical shape and the highest possible T_d symmetry. Only the A_1, E, and T_2 modes are Raman active based on the group theory. Thus, Raman intensities of A_1, E, and T_2 modes for each Si NC are calculated and shown in Figs. 6–8.

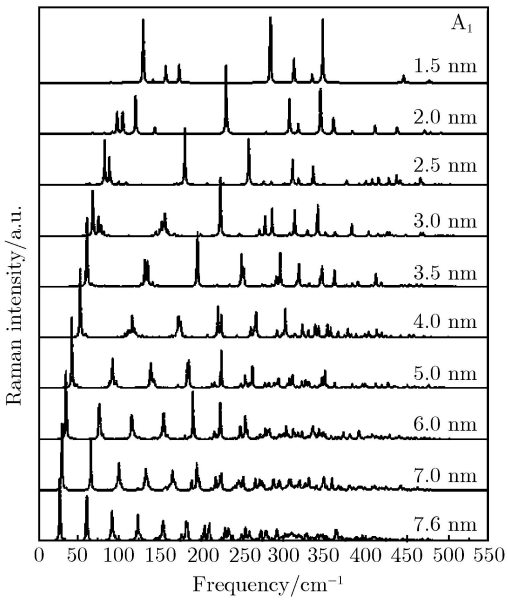

Fig. 6 Reduced Raman intensities of A_1 modes for Si NCs with approximate diameters in nm indicated.

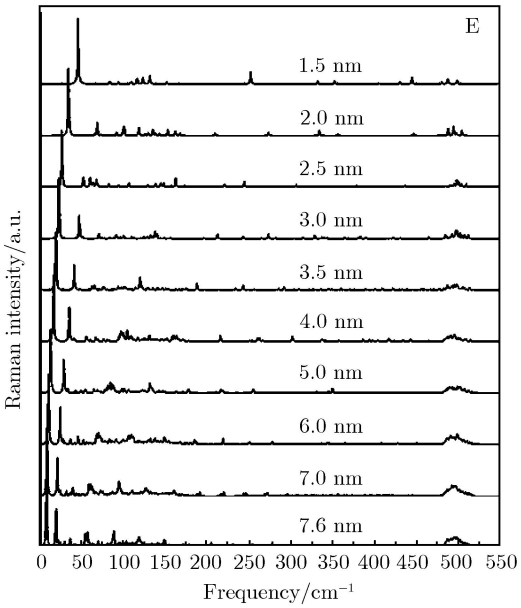

Fig. 7 Reduced Raman intensities of E modes for Si NCs with approximate diameters in nm indicated.

It is shown from Figs. 6 and 7 that the lowest frequency A_1 peaks decrease faster than E peaks as size increases, because A_1 modes have more quantum confinement effect. It is also found that the lowest frequencies of the Raman peaks in the acoustic range are roughly proportional to the inverse of the NC diameters, which was observed by Duval [35]. They are macroscopic spheroidal Lamb modes instead of torsional Lamb modes [16–18]. The group theory cannot tell the Raman activity differ-

ences between these two kinds of modes. The projection of microscopic modes to the macroscopic Lamb modes distinguishes Raman activity of the spheroidal and torsional Lamb modes [16–18]. The frequencies of macroscopic Lamb modes are proportional to the inverse of diameter [15]. Phonons of a large size NC are closer to those of a continuous sphere. In large size NCs, the Raman peaks are thus evenly spaced at the low frequency side of the spectra. In small size NCs, phonons are more different from the continuous model and the Raman peaks are not evenly spaced.

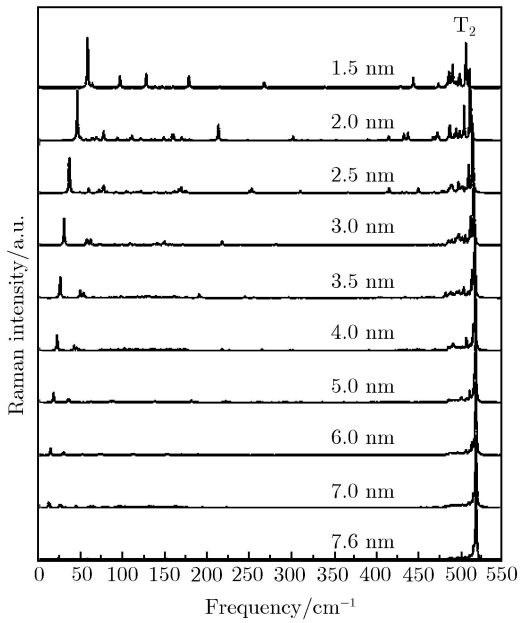

Fig. 8 Reduced Raman intensities of T_2 modes for Si NCs with approximate diameters in nm indicated.

It is seen from Figs. 6–8 that the highest frequency optical peak is caused by T_2 modes. When the size of NCs decreases, the frequency of this T_2 peak decreases. When the diameter of Si NCs decreases from 7.579 to 1.411 nm, the frequency of the highest Raman peak shifts from 518.3 to 506.4 cm^{-1}. The systematic red-shift of the longitudinal LO phonon peaks due to spatially confined phonon modes in NCs in the size range of a few nanometers has been observed [30–32], and it has been observed by resonant Raman scattering in three samples of Ge NCs in the size range of 4–10 nm [33]. One more observation from Fig. 8 for the high-frequency peaks is that not only do the highest intensity peak redshifts occur as NC size decreases, but weaker peaks also appear at the lower frequency side of the highest frequency optical peak at the same time. Experimentally, it may be difficult to resolve all the weaker peaks because of broadening from the fluctuation in dot sizes. As a result, one may observe an asymmetric broadening of the Raman peak corresponding to the optical phonon as the dot size is reduced [34]. This indicates that the observed broadening in Raman measurements is not only due to the red-shift of the peak alone, but also to quantum size effects.

Raman intensity per atom is also calculated [15]. Raman intensities of A_1 and E modes decrease as the size of NC increases. The same is true for low frequency T_2 modes, while those of high frequency T_2 modes are almost a constant independent of size. Thus, the Raman spectrum observed in the experiment is predominantly of T_2 optical modes for large size NCs.

The Raman intensities of Ge NCs with free surface follow similar rules as discussed for Si NCs. The Raman intensities of Ge NCs in a fixed surface are also calculated. Raman intensities of A_1 and E modes for fixed surface NCs are very small and can be ignored. Raman intensities of T_2 modes in the low frequency side can also be ignored. Raman intensities of T_2 modes in the high frequency side are close to that of free surface NCs when the size of NC is larger than 4.0 nm. However, redshifts are found for small size NCs with a free surface compared with those with a fixed surface [13]. Thus, NCs with a fixed surface are more like bulk materials in the Raman spectra. Major differences between the Raman spectra of the free and fixed surface suggest that the matrix effect is larger for NCs with size less than 4.0 nm, and Raman spectra in the low frequency side can also detect matrix effects in real NCs.

7 Raman intensities of Si_xGe_{1-x} alloy NCs

Raman intensities of Si_xGe_{1-x} alloy NCs can be approximated using PDOS. Since the alloy NC does not have a symmetry, all the phonon modes are Raman active. On average, the PDOS and Raman spectra share many similarities as shown below. We have plotted in Fig. 9 the experimental Raman spectra of SiGe alloy on top of the theoretical PDOS for comparable values of x. In making these comparisons we should keep in mind that the theoretical frequencies for the peaks identified as "Si-Si" and "Ge-Si" by Renucci *et al.* [28] (strictly speaking, the so-called Ge-Si peak is really due to Si atomic vibration as we have shown) will be slightly lower than those in the experimental spectra because of our approximation in using the Ge force constants for even Si atoms. In addition, our PDOS does not include the electron-phonon interaction necessary for calculating the intensity. Thus, our calculated dependence of Ge peak position on alloy concentration does not fully agree with that obtained

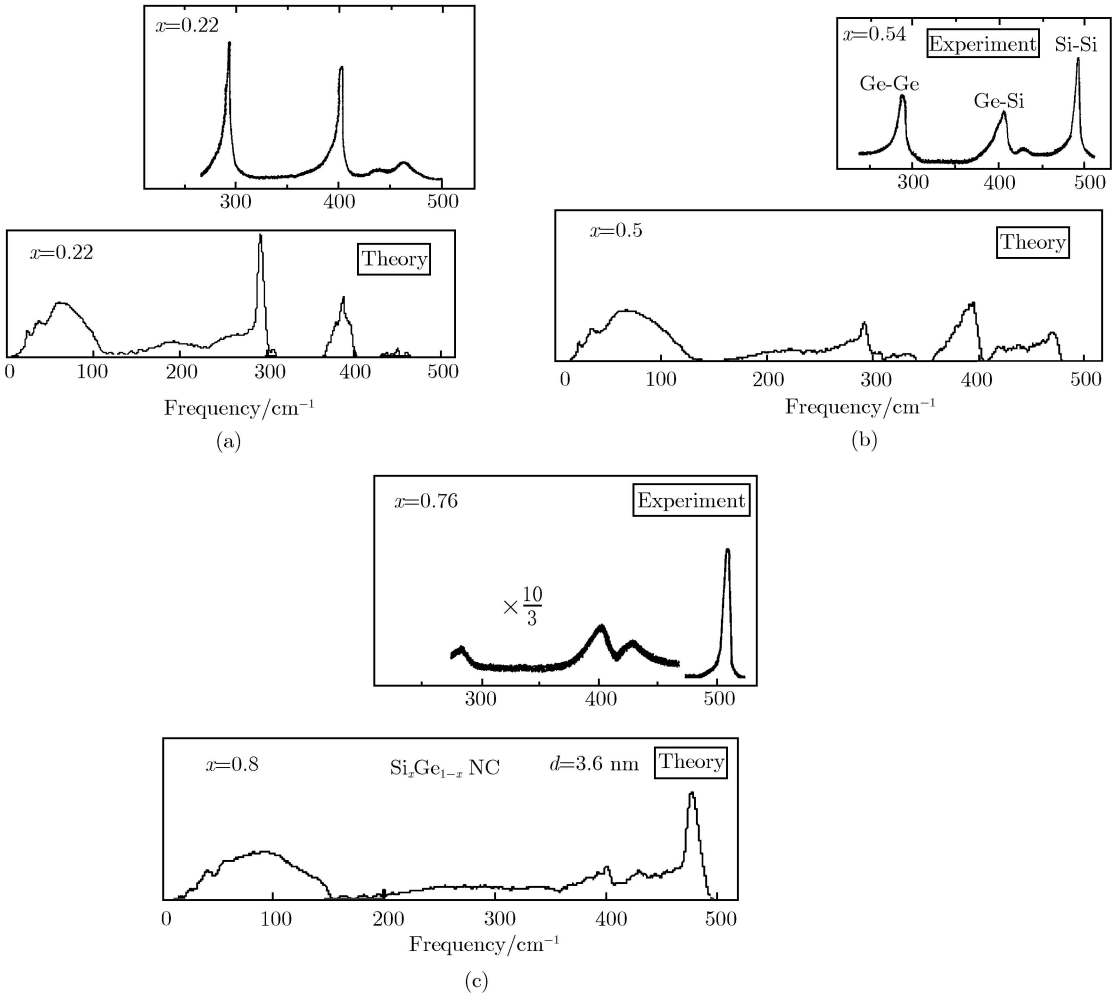

Fig. 9 Comparison between the theoretical phonon density-of-states (PDOS) calculated for NC and the experimental Raman spectrum in bulk SiGe alloy (Ref. [21]) with comparable Si concentration x for **(a)** x ∼0.2, **(b)** x ∼0.5, and **(c)** x ∼0.8.

by Renucci *et al.* [28] as discussed in Section 4. Otherwise our computed PDOS generally agrees quite well with the experimental Raman spectra shown in Fig. 9. For example, Renucci *et al.* [28] found that for x=0.54 and 0.76 the "Ge-Si" Raman peak broadened asymmetrically, while another broad peak appeared at 430 cm^{-1} and grew with x. Our calculations suggest that the peak at 430 cm^{-1} originates from the vibration of small Si clusters in the alloy, in which a Si atom is surrounded by one to three Si atoms. The width of this peak is caused by inhomogeneous broadening of the vibration frequencies resulting from the different configurations of these clusters. Our interpretation of this peak is thus different from the local phonon mode of a Si embedded in the $Si_{0.5}Ge_{0.5}$ alloy model proposed by Renucci *et al.* [28]. We also note that Tsang [20] has reported the Raman spectra of ultra-thin (less than 6 monolayers or ML) Ge film grown on a Si [100] surface. According to our model, the Si atoms at the film interface will have very well-defined local configurations: Each Si will be surrounded by two Si and two Ge atoms and therefore will be even narrower than the Si-Si_2Ge_2 spectrum shown in Fig. 5. Indeed, the experimental spectra for the 2–3 and 5–6 ML (Ref. [20]) show mainly one sharp peak without the higher energy tail due to the Si cluster containing more than two Si atoms in the nearest neighbor. On the other hand, the thinnest 1 ML Ge shows two broad peaks, indicating a lot of intermixing between Si and Ge atoms to form many clusters of different configurations. Such intermixing-induced broadening of the Ge-Si mode in experimental Raman spectra has also been reported in Ge/Si superlattice by Headrick *et al.* [21] and by Kwok *et al.* [22] in self-organized Ge quantum dots superlattice grown on Si substrates. When the superlattices are grown without a Sb surfactant layer, these authors found that the Si local phonon peak around 417 cm^{-1} exhibits

strong asymmetric broadening on the lower frequency side. Based on our calculation, this result can be explained by the infiltration of Ge atoms into the Si barrier layers producing Si clusters with three or more Ge atoms. As in the case of the ultra-thin Ge films [20], the Si local phonon peak in a perfect quantum dot film should be very sharp and results from the vibration of Si-Si_2Ge_2 cluster only. Figure 5 shows that the presence of clusters containing more Ge atoms such as Si-$SiGe_3$ produces additional modes mainly on the lower energy side of the Si local phonon.

8 Summary

In summary, we have investigated PDOS of Si, Ge, and SiGe alloy NCs with various sizes and two different types of surfaces by VFFM. Raman intensities are calculated. In the size effect of NCs we found the highest optical peak red-shifts as the size of NCs decreases. In the PDOS a peak at 211 cm^{-1} is found for fixed surface Ge NCs. In the alloy NC Si-Ge mode at 400 cm^{-1} is Si major localized modes. The observed broadening in Raman measurements is not only due to the red-shift of the optical peak alone, but also to quantum size effects.

Acknowledgements S. F. Ren acknowledges the support by Research Corporation (CC6274). W. Cheng acknowledges Illinois State University for hosting his research visit.

References

1. J. Ouellette, The Ind. Phys., 2002, 8: 22
2. A. D. Yoffe, Adv. Phys., 1993, 42: 173
3. A. D. Yoffe, Adv. Phys., 2001, 50: 1
4. A. D. Yoffe, Adv. Phys., 2002, 51: 799
5. G. A. Slack and M. A. Hussain, J. Appl. Phys., 1991, 70: 2694
6. C. B. Vining, Nature (London), 2008, 451: 132
7. S. F. Ren, W. Cheng, and G. Chen, J. Appl. Phys., 2006, 100: 103505
8. E. Roca, C. Trallero-Giner, and M. Cardona, Phys. Rev. B, 1994, 49: 13704
9. M. P. Chamberlain, C. Trallero-Giner, and M. Cardona, Phys. Rev. B, 1995, 51: 1680
10. C. Trallero-Giner, A. Debernardi, M. Cardona, E. Menendez-Proupin, and A. I. Ekimov, Phys. Rev. B, 1998, 57: 4664
11. W. A. Harrison, Electronic Structure and the Properties of Solids, San Francisco: Freeman, 1980
12. W. Cheng and S. F. Ren, Phys. Rev. B, 2002, 65: 205305
13. S. F. Ren and W. Cheng, Phys. Rev. B, 2002, 66: 205328
14. W. Cheng, S. F. Ren, and P. Y. Yu, Phys. Rev. B, 2003, 68: 193309
15. S. F. Ren, W. Cheng, and P. Y. Yu, Phys. Rev. B, 2004, 69: 235327
16. W. Cheng, S. F. Ren, and P. Y. Yu, Phys. Rev. B, 2005, 71: 174305
17. W. Cheng, S. F. Ren, and P. Y. Yu, Phys. Rev. B, 2005, 72: 59901
18. W. Cheng, S. F. Ren, and P. Y. Yu, in: AIP Conference Proceedings, 2005, Vol. 772: 851
19. W. Cheng, S. F. Ren, and D. T. Marx, in: Nanoscience in Biomedicine, edited by D. L. Shi, Chapter 20, Springer and Tsinghua University Press, 2008
20. J. C. Tsang, in: Light Scattering in Solids, edited by V. M. Cardonaand and G. Güntherodt, Topics in Applied Physics, Vol. 66, Berlin, Heidelberg: Springer, 1989: 233
21. R. L. Headrick, J. -M. Baribeau, D. J. Lockwood, T. E. Jackman, and M. J. Bedzyk, Appl. Phys. Lett., 1993, 62: 687
22. S. H. Kwok, P.Y. Yu, C. H. Tung, Y. H. Zhang, M. F. Li, C. S. Peng, and J. M. Zhou, Phys. Rev. B, 1999, 59: 4980
23. R. J. Bell, in: Methods in Computational Physics, edited by B. Alder, S. Fernbach, and M. Rotenberg, Vol. 15, New York: Academic Press, 1976: 260
24. D. J. Lockwood, K. Rajan, E. W. Fenton, J. -M. Baribeaue, and M. W. Denhoff, Solid State Commun., 1987, 61: 465
25. L. Vegard, Z. Phys., 1921, 5: 17
26. H. Lamb, Proc. London Math. Soc., 1982, 13: 189
27. L. Genzel, T. P. Martin, and C. H. Perry, Phys. Status Solidi B, 1974, 62: 83
28. M. A. Renucci, J. B. Renucci, and M. Cardona, in: Proceedings of the International Conference on Light Scattering in Solids, edited by M. Balkanski, Paris: Flammarion, 1971: 326
29. P. Y. Yu and M. Cardona, Fundamentals of Semiconductors, Physics and Materials Properties, 3rd Ed., Berlin, Heidelberg: Springer, 2003
30. P. T. C. Freire, M. A. Araujo Silva, V. C. S. Reynoso, A. R. Vaz, and V. L. Lemos, Phys. Rev. B, 1997, 55: 6743
31. Y. N. Hwang, S. Shin, H. L. Park, S. H. Park, U. Kim, H. S. Jeong, E. J. Shin, and D. Kim, Phys. Rev. B, 1996, 54: 15120
32. A. Balandin, K. L. Wang, N. Kouklin, and S. Bandyopadhyay, Appl. Phys. Lett., 2000, 76: 137
33. K. L. Teo, S. H. Kwok, P. Y. Yu, and S. Guha, Phys. Rev. B, 2000, 62: 1584
34. P. Y. Yu, private communication
35. E. Duval, Phys. Rev. B, 1992, 46: 5795